Fabrication and Characterization of Metal- Insulator -Metal Diode and Gray scale Lithography

by

Manal Alhazmi

A thesis
presented to the University of Waterloo
in fulfillment of the
thesis requirement for the degree of
Master of Applied Science
in
Mechanical Engineering-Nanotechnology

Waterloo, Ontario, Canada, 2013

AUTHOR'S DECLARATION

I hereby declare that I am the sole author of this thesis. This is a true copy of the thesis, including any required final revisions, as accepted by my examiners.

I understand that my thesis may be made electronically available to the public.

Abstract

The objective of this thesis is to successfully design, fabricate, and characterize an optimum metal-insulator-metal diode that can be used as a fast switching diode in various applications such as solar energy conversion. The improvements of this type of diode will result in rectification of a wider spectrum of AC signals to usable electricity. In this project, several proposed designs of MIM diodes were successfully fabricated and characterized. Pt-Al_2O_3-Al metal-insulator-metal diode was fabricated to have high asymmetry in I-V curve. Additionally, in an attempt to study the effect of material properties on MIM diode's performance, four different combinations of MIIIIM diode were compared and discussed. Many processes were involved in the fabrication of these diodes such as E-beam evaporation, photolithography, reactive ion etching RIE, and Atomic Layer Deposition (ALD) technique. The fabricated tunneling diodes are intended to operate in the GHz regime and can also operate at higher frequencies (THz) by changing and scaling the dimensions.

In addition to MIM diode work, this project attempted to engineer the contrast curve of polystyrene as a negative resist used for E-beam lithography using multi layer resist stack. If the resist stack has a very high contrast and its sensitivity differs between the various layers, it can be ideal for the fabrication of multi-level zone-plate/Fresnel lens.

Acknowledgements

Words are not enough to thank my supervisor, Professor Mustafa Yavuz, whose continuous encouragement and attention guided me and made this work possible. I also wholeheartedly thank my co-supervisor Professor Bo Cui for his energetic work in assisting me during my laboratory training, as well as in all matters at all times.I offer special thanks to my colleague Ferhat Aydinoglu as well as my group members for their cooperation in facilitating all challenges I encountered. With great pleasure, I thank G2N lab technicians Richard Barber and Robert Mullins as well as all G2N lab users for their help in carrying out my experiments smoothly. I give warm thanks to my parents and family members for their prayers and encouragement that helped me in accomplishing this work. I am highly indebted to my husband Khalid for his support and motivation that enabled me to undertake my higher education.

Dedication

To my great parents, my beloved husband Khalid, and my family

Table of Contents

List Of Figures

List Of Tables

Chapter 1

Metal-Insulator-Metal Diode

1.1 Research Motivation

There is still a continuous need to develop devices, which can be used for energy harvesting without suffering from issues such as low harvested current and high cost. Rectenna (antenna coupled with a rectifying element) has attracted attention over the last few years due to its powerful efficiency in harvesting energy compared to previous methods such as solar cells. As the rectifier used in rectennas is the most important part of this system, any improvement in this aspect will lead to a huge development in the rectenna system. Metal-insulator-metal diode is the best candidate for rectification in rectenna devices because of its fast response time and high efficiency in converting alternating current to direct current. Therefore, over recent years various research groups have tried to develop MIM diode in order to enhance the rectification process of the electromagnetic radiation.

1.2 Overview of MIM Tunnel Diode

Metal-insulator-metal diode is a significant device since it has a large number of applications in electronic devices, including energy harvesting systems, infrared photo detection, and switching devices. For the purpose of energy harvesting, this device is used to convert solar electromagnetic radiation (alternative current) to direct current in a circuit. MIM diode consists

of two electrodes and an ultra-thin insulator layer between the two electrodes. Even though MIM diode is considered an optimum diode used as a rectifier in rectennas, its fabrication is still challenging.

MIM diodes are based on the quantum tunneling theory; thus, their basic structure requires two electrodes divided by a thin barrier in order to allow current to flow according to the tunneling phenomenon [10]. In MIM tunneling diodes, the electrons flow between the two metal electrodes via a thin insulator layer. Exploiting this concept has led to a reliable rectification in microwaves for critical emerging energy harvesting applications.

1.3. Tunnel Junction Theory

Metal-insulator-metal (MIM) tunnel junctions have been proposed for over four decades and have led to several key studies in condensed matter physics, including the Josephson Effect. In the MIM diode, two dominant phenomena - thermionic emission and quantum mechanical tunneling - achieve the rectification of electromagnetic radiation induced by the antenna. The thickness of the insulator is an important factor for rectification. In other words, the smaller the thickness of insulator layer, the higher current delivered. For example, in case of thicknesses less than 4nm, rectification is primarily achieved through tunneling. Alternatively, for thicknesses more than 4nm, either tunneling or thermionic might predominate depending on the barrier height. Asymmetry of MIM diode can be improved by using two different electrodes with different work functions and density of states. It is preferred that these two electrodes are metal in order to maintain high conductivity. Achieving conduction by tunneling mechanism would result in ultrafast response time.

1.4 Methodology and Characterization Tools

In this thesis, various lithographies and nanofabrication techniques have been utilized to carry out the project's experiments. Fabrication techniques included photolithography, electron-beam lithography, electron-beam evaporation, atomic layer deposition (ALD), spin coating, and nanoimprint lithography. Characterization was achieved using atomic force microscopy (AFM), scanning electron microscopy (SEM), and keithley 4200-SCS-semiconductor characterization system connected to a probe station.

1.4.1 Photolithography

Photolithography is a main process in micro fabrication used to transfer patterns onto the substrate. Exposing a photosensitive material to a light field like ultraviolet radiation transfers the desired pattern. The photosensitive material is usually an organic polymer, which is called photoresist. Simply, the photoresist is spin coated onto the substrate surface. By using the spin coating process, a uniform layer of the photoresist is achieved. Following spin coating, the substrate is baked to ensure that no solvents remain. This photoresist is then exposed to ultraviolet radiation through a photo mask. Photoresist material can have either a positive tone or a negative tone; the difference arises from how light influences them. The positive tone of the polymer is insoluble in the resist developer; however, the negative tone is soluble, as shown in Figure 1.1.

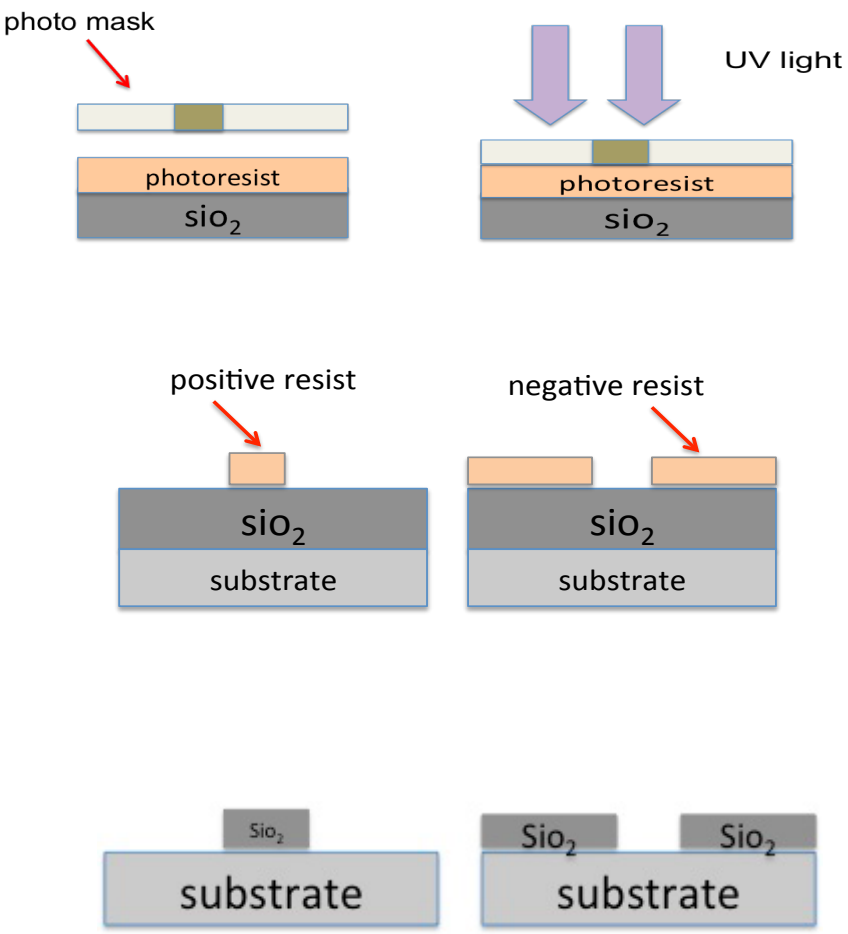

Figure 1.1 Schematic representation of photolithography process using positive and negative resist

1.4.2 Nanoimprint Lithography

The first proposed replication process was nanoimprint, which relies on heat and press. Unlike a hot embossing process that relies on heat and press but is used for microstructure, nanoimprint process is used to replicate structures in nano scale.

The basic procedure of nanoimprint is illustrated in Figure 1.2. First, a thin layer of polymer is coated on a substrate and then heated above its transition (Tg) temperature to approximately 50 ℃–100 ℃. The objective of heating the polymer film is to make it become softened. At a pressure of approximately 50-100 bars a surface relief stamp is then pressed into the polymer film. Pressure value could be adjusted depending on viscosity of the molten polymer. Typically, pressure is released at 108 ℃. and the stamp is separated from the imprinted sample after it cools down. Various key factors need to be considered for replication in sub 100nm features including the polymer, the stamp, alignment if multi imprinting is needed, and demolding. The final step removes the residue of the polymer using reactive ion etching RIE [19].

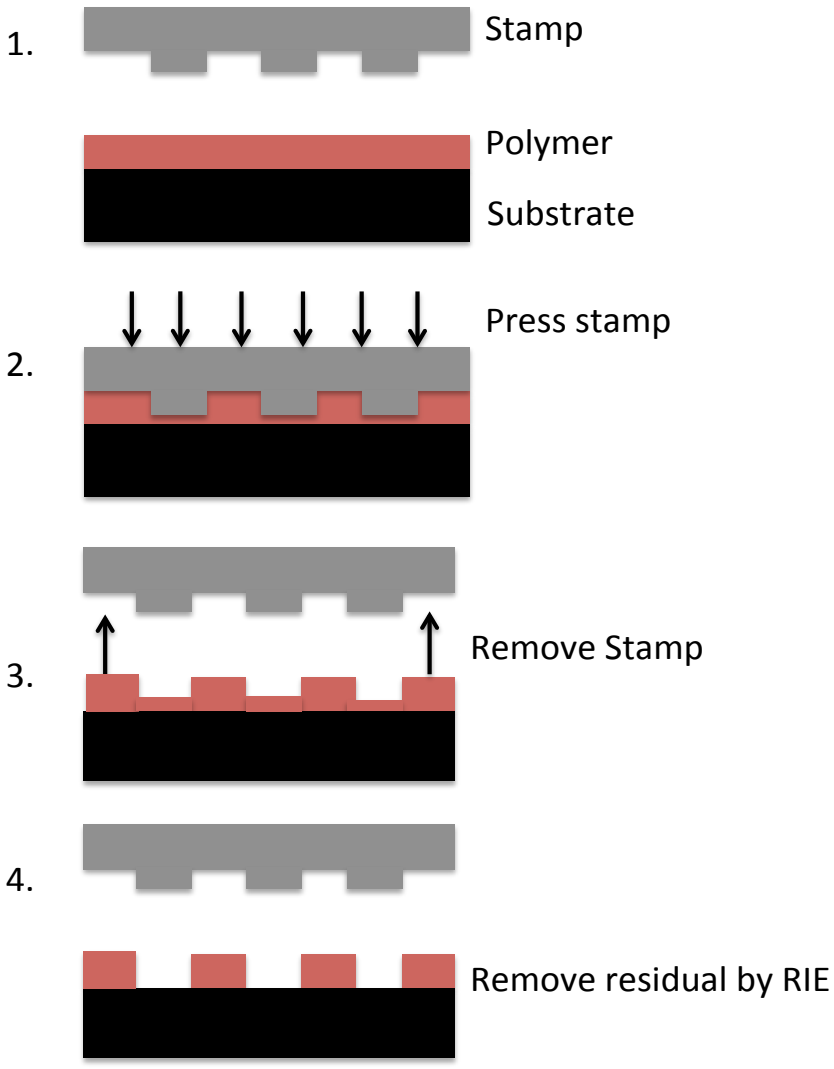

Figure 1.2 Schematic illustrations for nanoimprint process

1.4.3 Electron-beam Evaporation

In the electron beam evaporation process, a focused beam of electrons is used to heat and evaporate metals. The temperature of these electrons can be approximately 10,000K, and they are accelerated by DC 10kV. Evaporation occurs near the beam bombardment spot on the source surface at a highly localized point.

1.4.4 Scanning Electron Microscopy (SEM)

Scanning electron microscopy (SEM) is used to determine the crystal structures of the specimen. Different signals are generated in SEM system, including secondary electrons (SE), backscattered electrons (BSE), and diffracted backscattered electrons (EBSD). Figure 1.3 shows the SEM detection mechanism.

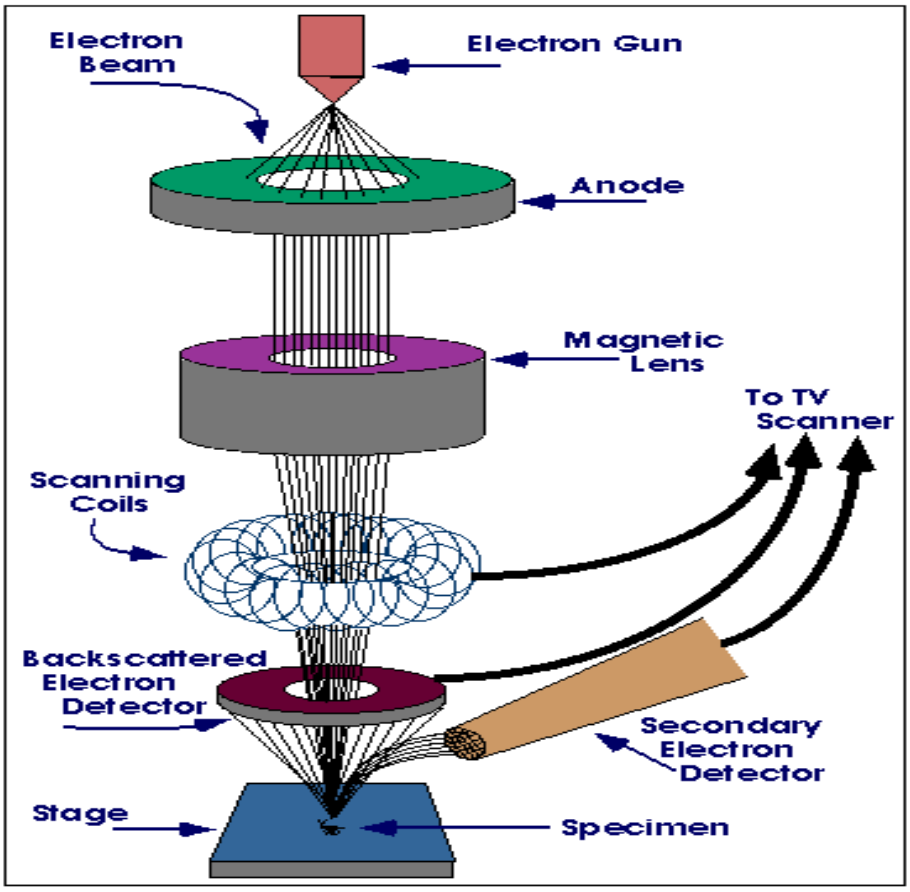

Figure 2.3 Detection mechanism of scanning electron microscopy (SEM) [18]

Secondary electrons are produced from primary electrons and used for imaging as the near surface SE extends to reach the detector. The morphologic and topographic properties of the specimen can be demonstrated from detection of secondary electrons[18]. On the other hand, backscattered electrons can identify different phases of the internal structure of the sample as

they reveal the small variations of the atomic number on the sample surface by providing different contrasts in image. These backscattered electron signals (BSEs) are widely used for the investigation of specimen surface [20, 21]. The mechanism of the interactions between incident beam and sample surface are shown in Figure 2.3 [18] .

1.4.4.1 SEM Images

Several SEM parameters should be adjusted in order to obtain a high quality image. One such parameter is the working distance, which is known as the distance between the bottom pole piece of the objective lens and the sample surface. The working distance affects depth of focus (D), expressing the range of depth that an image appears to be in focus. The following equation is used to determine the depth of field:

$$D = 2r \times WD/R$$

Where r is the maximum radius of the beam, WD represents the working distance, and R is the final aperture radius.

Using a lower accelerating voltage can be beneficial for obtaining good SEM image quality and finer surface structure images. In contrast, applying higher accelerating voltages could reduce the image contrast. The reason behind minimized contrast is the unnecessary signals from the large penetration and diffusion area. Figure 1.4 shows the effects of accelerating voltage on a sample composed of heavy or light elements [23].

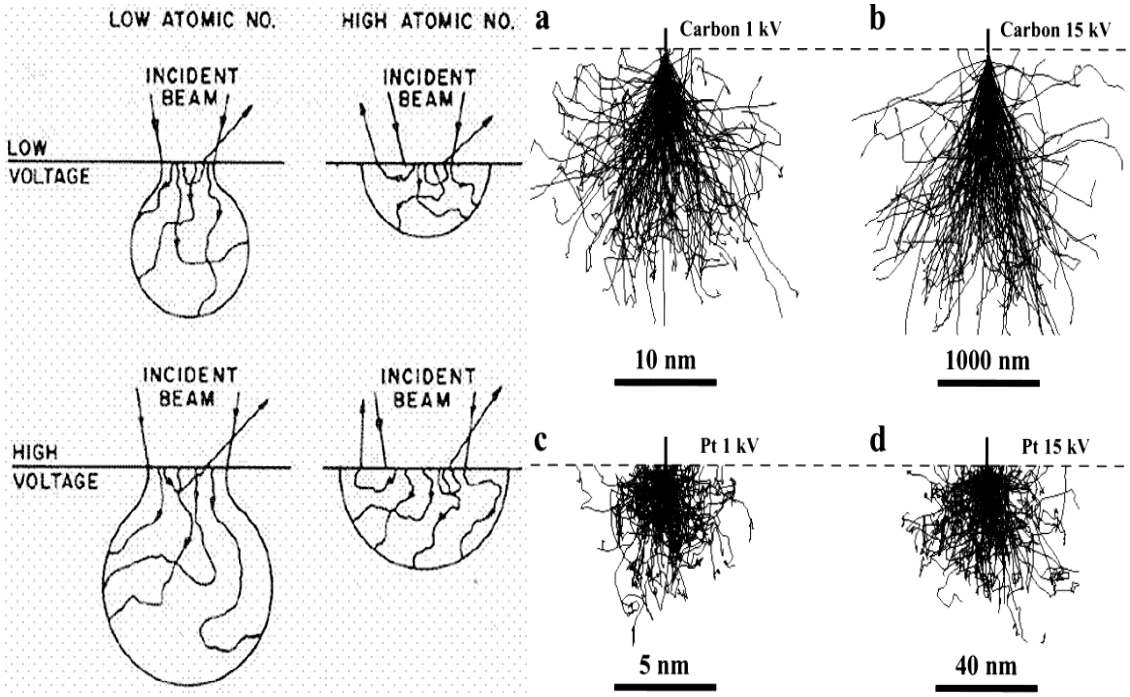

Figure 1.4 Accelerating voltage effects on interaction of sample composed of heavy or light elements [23]

Chapter 2

Design and Fabrication of MIM Diode

2.1 Design and Fabrication of Pt-Al_2o_3-Al Metal-Insulator-Metal Diode

In this work, a Pt-Al_2O_3-Al metal-insulator-metal diode was fabricated to have high asymmetry in I-V curve. The fabricated tunneling diode is intended to operate in the GHz regime, and can also operate at higher frequencies (THz) by changing the dimensions. The asymmetry of the I-V curve is reasonably very high due to a large difference in the work function between Aluminum and Platinum metals.

2.1.1 Introduction

Investigation of new energy sources is vital because of the increasing demand for energy [3]. These new energy sources should be more efficient, cleaner, safer, and cheaper than traditional energy sources. The solar energy based devices are clean and safe, but they are not efficient enough, and at the same time they are expensive compared to fossil fuels and nuclear energy. Efficiency of traditional solar cells is limited because of the band gap of semiconductors used in these cells. This issue along with the huge amount of radiation received from the sun have led researchers to investigate new technologies for converting solar energy to electricity. One energy-harvesting device used in these systems is a rectifying antenna, also called a rectenna, which converts solar radiation directly to electricity. The rectennas consist of an antenna, a rectifier system, and frequency filters. The rectifier plays the primary role in converting AC

signals to direct current (DC), which can then be used directly or else used to charge batteries. The cut-off frequency of the diode should be high enough to respond and be compatible with the electromagnetic energy that is being harvested. Tunneling diodes are highly suitable for rectification in microwaves and THz regimes (and beyond) because of their fast response time. Metal-insulator-metal (MIM) diodes are one of the tunneling diodes used for rectification at high frequencies [4].

MIM diode consists of two electrodes and a thin dielectric layer sandwiched in between the electrodes [5]. Although this type of diode is considered an optimum diode used in rectennas, challenges remain in terms of its fabrication.

Rectennas consist of an antenna, filter circuits, and a rectifier diode. These devices have been used for lower microwave frequencies; however, there is a growing interest in harvesting energy in the infrared and optical frequency regimes [3, 5, 6, 7, 9]. In this study, the fabrication process of MIM diode will be discussed along with some challenges related to the fabrication process.

Some parameters including I-V characteristics, asymmetry, non-linearity, sensitivity, coupling efficiency, and response time are important for determining the diode's efficiency. The current density highly depends on the work function of the metals, electron affinity of the insulators, and thickness of the insulator layer. To have an efficient tunneling, the insulator layer should be ultra-thin (less than 10 nm). Additionally, for operating a MIM diode at high frequencies the contact area between the insulator and the metal interface should be very small; i.e., the contact area at visible light range should be approximately 20 nm x 20 nm. It is very difficult to have these ultra-small structures using current technology. In the next section, Pt-Al_2O_3-Al metal-insulator-metal diode will be discussed.

2.1.2 Design and Fabrication

The area of the diode is an important parameter that determines the operation frequency of the diode. The area and the frequency are related according to the following equations:

$$f_d = \frac{1}{2\pi R_a C_d} \qquad (1)$$

$$C_d = \frac{\varepsilon_0 \varepsilon_r A_d}{d} \qquad (2)$$

Where R_a is the antenna's resistance, C_d is the diode capacitance, and A_d is the diode area [6, 10]. The design of this diode is a simple structure of four layers on top of the Si substrate. Ti, Pt, and Al were the materials chosen for this diode.

For operation at 3GHz, the dimensions of the diodes were chosen to be 5 μm x 5 μm by using Equations 1 and 2. The resulting Ra is 100Ω, which is close to a typical antenna resistance. The thickness of the insulator was chosen to be 4 nm to have efficient tunneling. Although these kinds of diodes are used for high frequency (near-IR or visible range), the frequency range was not considered since the aim was to have high asymmetry in I-V curve.

Many processes were involved in the fabrication of the Pt- Al_2O_3 -Al MIM diode including E-beam evaporation, photolithography, reactive ion etching RIE, and Atomic Layer Deposition (ALD) technique. The AFM was used to verify the smoothness of the surface of the diode and the thickness of Al pads.

a)

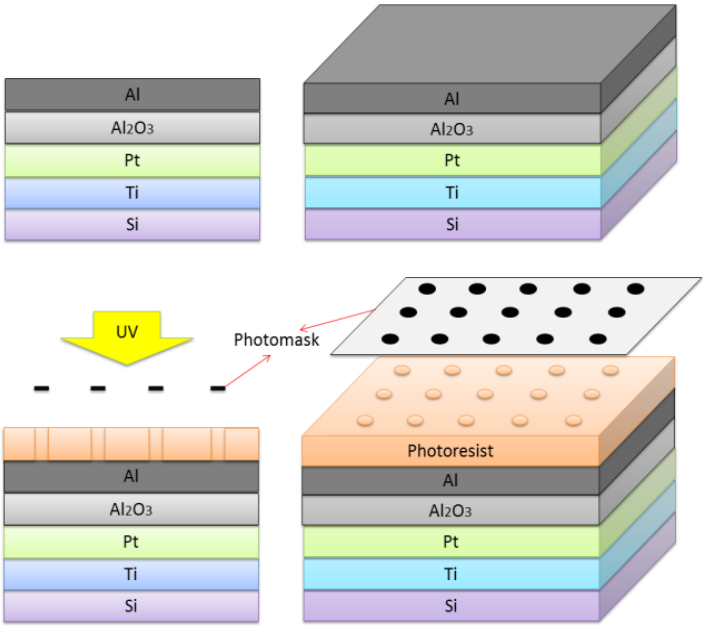

b)

Figure 2.1 A schematic representation of the fabrication flow steps of the diode: a) Deposition of Ti/Pt/Al_2O_3/Al; b) Patterning

The substrate of the diode was chosen to be a bare silicon wafer. The selected materials used as the top and bottom electrodes were Platinum and Aluminum, respectively. These materials were chosen due to their high difference in work function. They were good candidate metals for the diode. The work function of Pt is 5.65 eV and that of Al is 4.28 eV. Electron-beam evaporation was then used to deposit 50 nm of Ti onto the Si wafer in order to increase the

adhesion of the Pt layer to the substrate. Next, ultra thin layer (4 nm) of aluminum oxide (Al_2O_3) was deposited onto the Pt layer using Oxford Plasma Lab 100 FlexAL ALD. It is preferred to deposit insulators using ALD rather than oxygen plasma technique, as ALD is more precise and controllable.

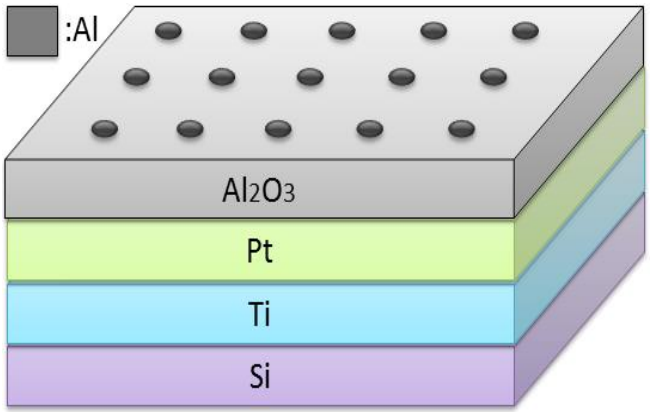

Figure 2.2 A schematic representation of the complete diode

Next, a 50 nm Al was deposited onto the insulator layer. Figure 2.1(a) shows the schematic of the structure up until this step. A positive photoresist (S1813) was spin coated onto the ARC under layer prior to photolithography. The conditions of the spin coating process were 2000 rounds per minute for 40 seconds followed by one minute soft baking at 110 ℃.

To carry out photolithography process, Karl Suss MA6 Mask Aligner was used. A glass photo-mask with 5-micron diameter dots and 20 micron spacing was used to pattern the device, as shown in Figure 2.1(b). The type of exposure was soft contact and G-line was chosen to expose the substrate for five seconds. Following the development of the photoresist in AZ 300 MIF developer for one minute and etching the ARC by Reactive Ion Etching (RIE), Oxford Instruments ICP380 plasma-based dry etching system was used to apply dry etching onto the Al

layer. A Laser End Point system connected to RIE was used to minimize the exposure of the Platinum. The sample was then soaked in acetone in order to clean the photoresist on the top followed by a four minute RIE process to clean the rest of the ARC by oxygen plasma. Figure 2.2 shows the final schematic of the device.

2.1.3 Results and Discussion

An important property of MIM diodes is the asymmetry in their I-V curve. This can be achieved by having different metals in both sides of the insulator; however, this will result in a high barrier asymmetric diode, which is good for having a large responsivity. Another property of MIM diode is low resistance, which requires a low barrier height [1]. A significant point that needs to be considered prior to fabricating MIM diode is the selection of metals, since the work function must be different to ensure asymmetrical and nonlinear characteristics of the diode. The asymmetry can basically be described as the magnitude of the ratio of forward (IF) to reverse bias (IR) current, as given by Equation 3.

$$F_{ASYM}=|I_F/I_R| \qquad (3)$$

Keithley 4200-SCS Semiconductor Characterization System, which was connected to a probe station, was used to obtain current versus voltage (I-V) curve. One probe was connected to the top of one of the Aluminum dots; another probe was connected to the Platinum surface. The current was measured from -1 Volt to +1 Volt applied bias. As shown in Figure 2.3-a, the I-V curve is highly asymmetrical. By using Equation 3, the asymmetry of the curve was plotted and shown in Figure 2.3(b). The value of the asymmetry reaches approximately 240 when 1 Volt bias is applied. A high asymmetric and non-linear I-V curve is illustrated in this study. However,

other parameters including tunneling efficiency, resistance, and responsivity should be considered during design and fabrication of these diodes.

To achieve high responsivity at zero bias, the barrier heights of the electrodes should be high. In our study, we used metals that have high work functions. Hence, the responsivity is also expected to be high. To obtain efficient quantum tunneling, the insulating layer should be as thin as possible; however, by using thick insulator layers, higher non-linearity can be achieved. To achieve low resistance, the barrier heights of both sides should be low and the insulator layer should be thin enough [11]. However, there are always some trade-offs in this concept. By using a thin insulator layer, a high non-linear and high asymmetric I-V curve was achieved in this study.

a)

b)

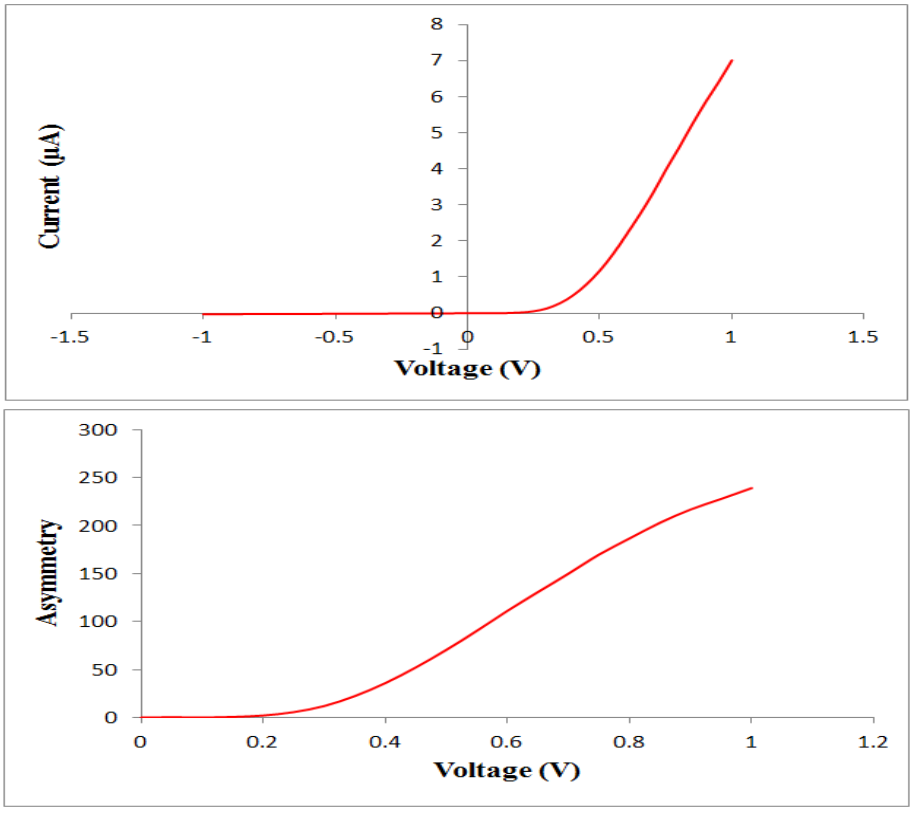

Figure 2.3 a) I-V curve; b) Asymmetry of Pt/Al_2O_3/Al MIM diodes

2.1.4 Conclusion

In this study, the fabrication of Pt-Al_2O_3-Al MIM diode was discussed in detail. In order to increase the frequency of MIM diode operation, the capacitance values should be small. This can be achieved either by increasing the thickness of the dielectric layer or by decreasing the contact area. Therefore, in this work the thickness of the insulator layer was chosen to be 4nm. The current-voltage characteristics of the fabricated diode are perceived to be sufficient for the diode to work at the GHz regime. The value of the asymmetry was measured as approximately 240 at 1 Volt, which represents highly asymmetric and non-linear I-V curve as seen in Figure 2.3(a).

2.2 Comparison of the Effects of Various Materials Properties on Metal-Insulator-Metal Diodes

This study compares various metal-insulator-metal diodes using the same bottom electrode but different top electrodes. New metal-insulator-metal diodes were fabricated with four insulators using various materials. Chromium was chosen for the bottom metal electrode while Ti, Cr, Al, and Pt were chosen for the top metal electrode. This work indicates the effectiveness of choosing the top metal for MIIIIM tunneling junction and its effect on the diode performance.

2.2.1 Introduction

The demand for using a sufficient and clean source of energy is continuous. Therefore, investigation of a fast response time rectifying element is essential to overcome the issue of having insufficient rectification[1]. The best candidate rectifying diode is metal-insulator-metal diode due to its advantages over semiconductor solar cells in terms of response time[7]. Metal-

insulator-metal diode is a junction consisting of thin insulating layer (less than 10nm) between two metals [1, 3, 6]. Even though the architecture of this diode is simple, it is still a challenge to determine which material's properties are most suitable for producing the preferable electrical performance of this device. Here, a comparison is provided of four different metal-insulator-metal diodes with multi-layers of insulators by changing the top metal electrodes and keeping the bottom one fixed. This comparison is based on the I-V characteristics and asymmetrical curves of the fabricated diodes. Materials chosen for the top electrodes were Ti, Cr, Al, and Pt. I-V characteristics are discussed in the next sections.

2.2.2 Experimental Details

Silicon oxide was the substrate chosen for all of the fabricated diodes to prevent the conductivity of the substrate during electrical measurements. In fabrication of Cr-Tio_2 -Al_2o_3 -Cr, Cr-TiO_2- Al_2O_3-Al, Cr-TiO_2- Al_2O_3-Pt, Cr-TiO_2- Al_2O_3-Ti MIIM diode, it was intended to keep the first metal and insulator layers fixed while changing the second metal electrode. Chromium was used as the fixed metal electrode, and chromium, aluminum, platinum, and titanium were chosen for the second electrode. The substrate was cleaned by acetone and isopropanol alcohol (IPA) and then dried by nitrogen blow. First, the negative photoresist (AznLOF 2035) was spin coated onto the SiO_2 substrate with 2000rpm spin speed for 40 sec, and then soft baking at 110°C was applied to the sample for one minute to ensure that there were no remaining particles of solvents. Following photoresist coating, Karl Suss MA6 Mask Aligner was used to pattern the diode through photolithography process. The photo mask was designed with different structures in different diameters. Following exposure, the substrate was baked at 110°C to allow for cross-

linking of the photoresist to occur. Next, the sample was developed by AZ300MIF developer for one minute and rinsed by IPA followed by DI water for one minute and then dried with N_2 gun.

Electron-beam evaporation technique was used to deposit 60nm of chromium. ALD technique was utilized to deposit TiO_2 and Al_2O_3, respectively. These two insulators were repeated in order to obtain a total number of insulators of four. Each insulator was 0.75nm thick, giving a total of 3nm barrier thickness. In fact, using ALD is an effective way to deposit a uniform layer of insulators due to its preciseness and controllability. Moreover, having a very uniform insulator is good for current flow. Another photolithography step was applied to the same sample in order to align the square's structure and complete the whole device. The second metal was then deposited with approximately 100nm thickness using electron-beam evaporation technique. The whole device's structure is clearly shown in Figure 2.4, and the overlapping area of metals one and two is shown in Figures 2.5 and 2.6.

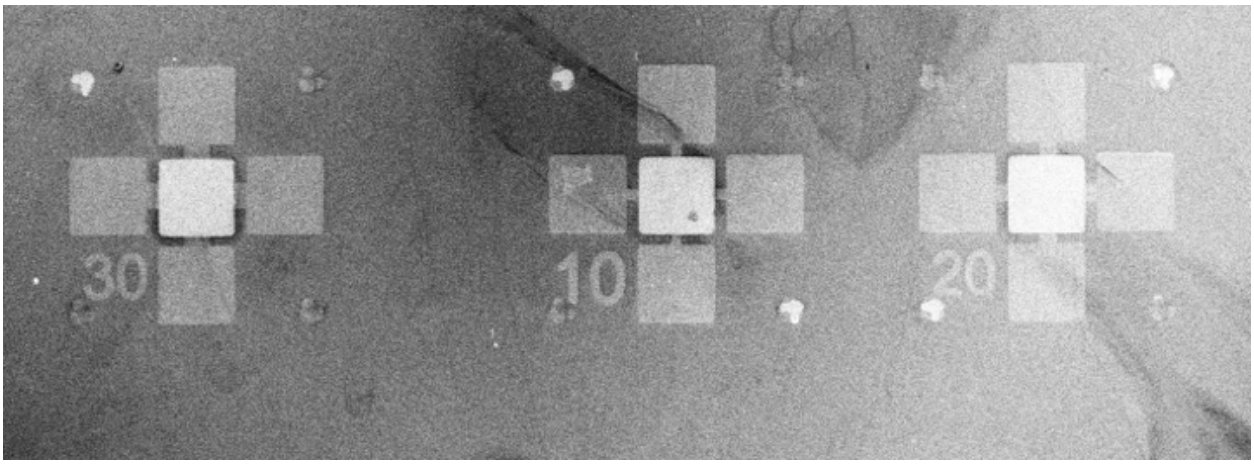

Figure 2.4 SEM image of the device structure showing three different sizes of the overlapping area (30, 20, and 10 micron)

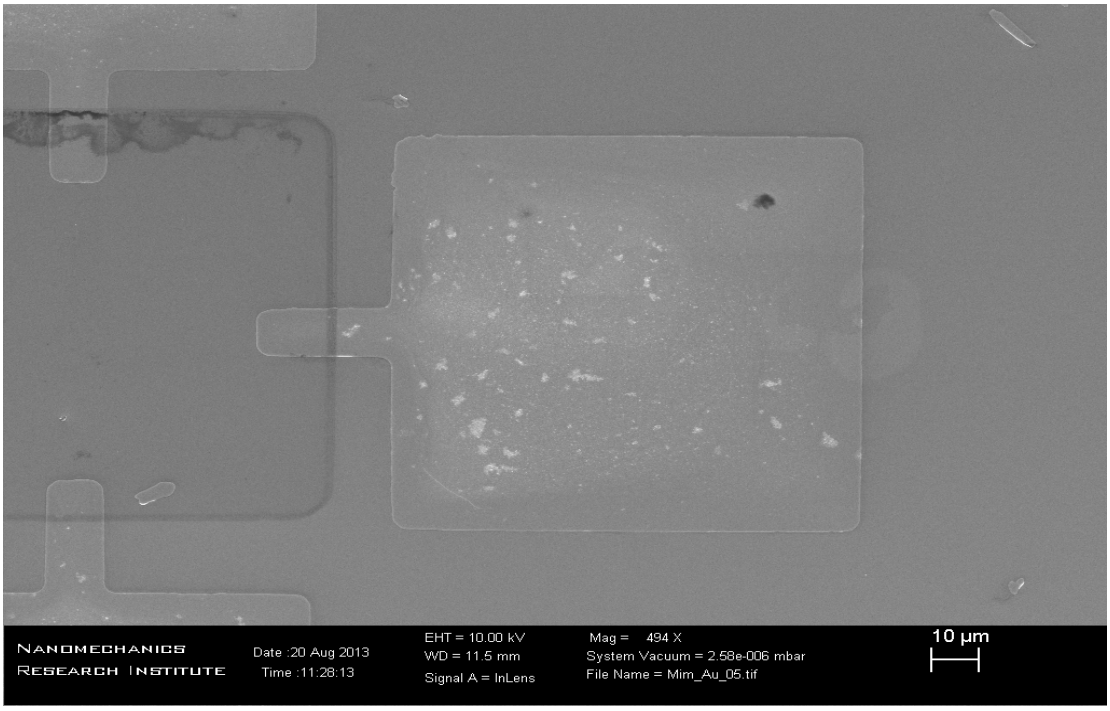

Figure 2.5 SEM image of the (Cr-TiO_2- Al_2O_3-TiO_2- Al_2O_3-Ti) diode structure

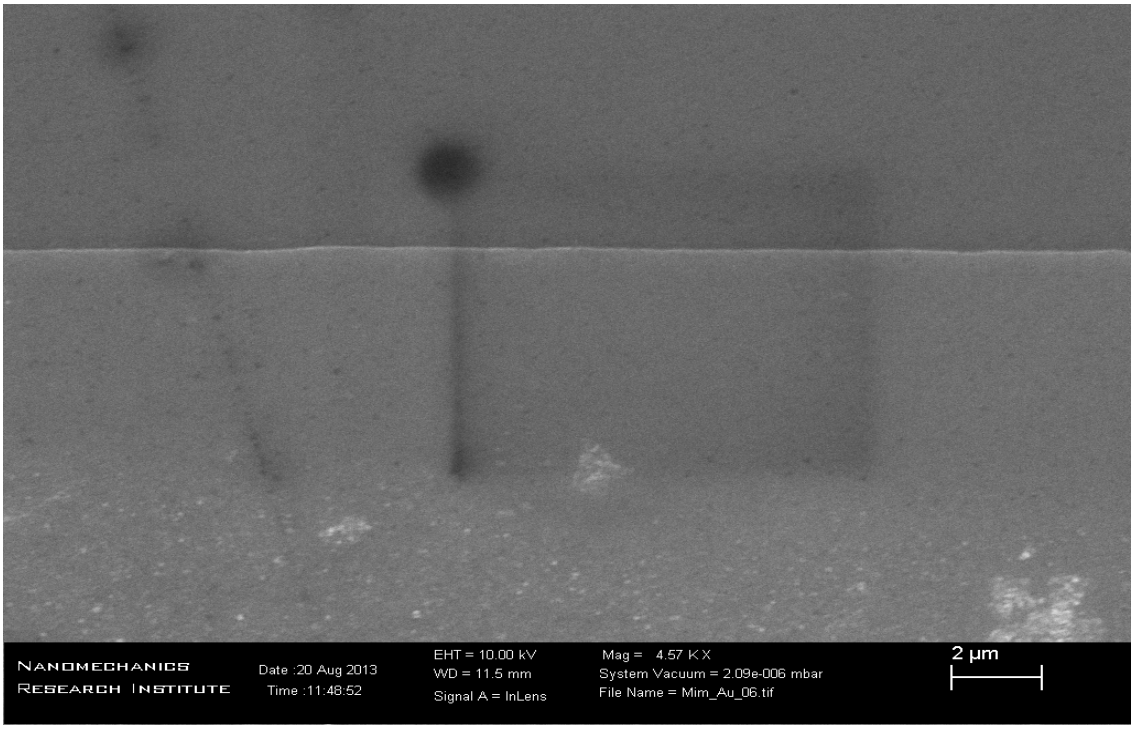

Figure 2.6 SEM image of the overlapping area (diode active area)

2.2.3 Results and Discussion

In order for MIM diodes to have optimal behaviour, the insulator layer requires a low surface roughness, uniform thickness, and stoichiometry. This can be obtained by having a small device area (in the order of μm^2 or less) [4]. Four combinations of MIM diode with different work function $\Delta\,\varphi$ (= $\varphi\,2 - \varphi\,1$) values were fabricated and characterized. The work function of chromium as the base metal is 4.5eV(φ_1). To improve the device's performance, a quadra insulator diode was fabricated using repeated TiO_2 and Al_2O_3 insulator layers. The same quadra insulator diode was repeated but with the second metal changed in order to study the difference between different material properties on the metal-insulator-metal diode. Each insulator layer of this quadra insulator layer diode was 0.75nm thick. These insulators were deposited by using ALD at a rate of 0.105 ± 0.001 nm/cycle for Al_2O_3 and a rate of 0.0437 ± 0.001 nm/cycle for TiO_2.

Figure. 2.7 shows the current-voltage electrical response for all the fabricated diodes having doubled insulator (red curve) and four insulators (blue curve). It is clearly shown that current resulted from diodes with four insulators is much larger than that of two insulators. When the device is forward biased, the electrons tunnel via the aid of a quantum well formed due to the insulator barrier, however, when a reverse biase is applied there is no quantum well formation occur and thus electrons must tunnel through all barriers without any assistance[2]. Therefore a highly nonlinear and asymmetric I-V curve results. Since there is a trade off between conductivity and nonlinearity, it is hard to achieve both, and hence devices with two insulators exhibited more nonlinear curves however conductivity is higher for devices with four insulators as shown in figure 3. From this figure also, it is clear that the MIM diodes using Ti and Cr, and

Pt as top electrodes perform most asymmetric diodes. This could be attributed to their band energy offset at the interface, which affects the tunneling current through insulating layers.

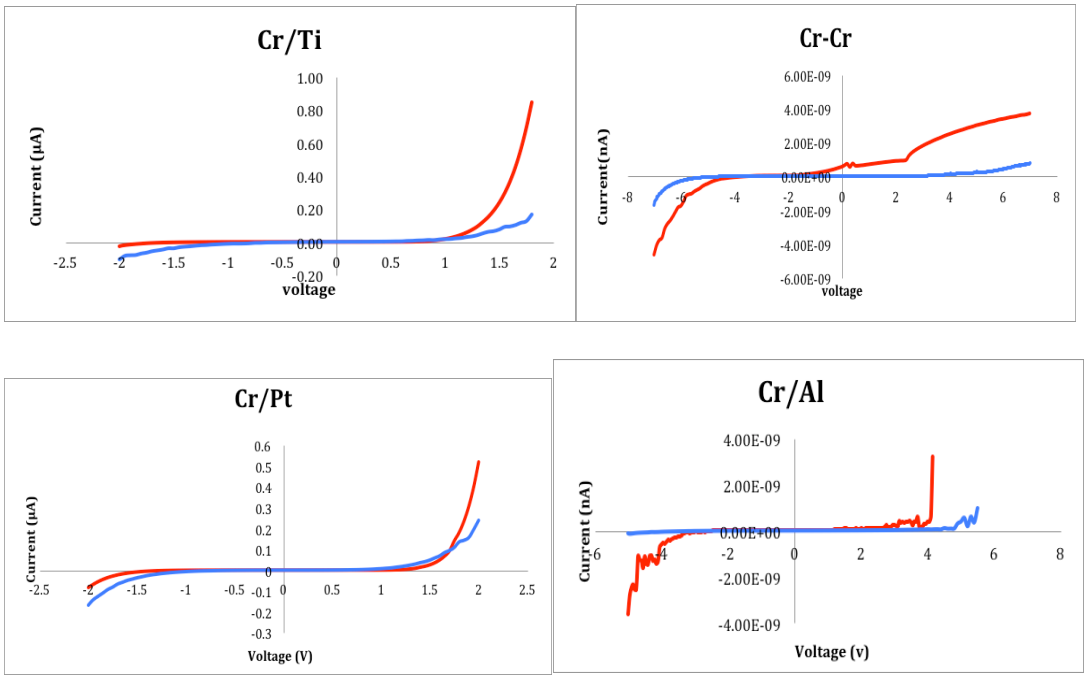

FIG.3. The I-V characteristics curve of the a) Cr-$I_1I_2I_1I_2$ .Ti and Cr-I_1I_2-Ti , b) Cr- $I_1I_2I_1I_2$. Cr and Cr- I_1I_2-Cr, c) Cr- $I_1I_2I_1I_2$-Al and Cr- I_1I_2-Al, and d) Cr- $I_1I_2I_1I_2$-Pt and Cr- I_1I_2-Pt diode.

Figure.2.8 compares the asymmetry curve of MIIIIM / MIIM fabricated diodes when a voltage range of (0.5-3 volts) is applied to these devices. . As can be seen from this figure the highest asymmetry value (40) was achieved at a voltage value of 1volt when using Ti as top electrode for the MIIIIM structure (blue curve), but for MIIM structure (red curve) it shows less asymmetry. When using the Pt as top electrode the asymmetry was calculated as 6 under 0.5 voltage, and much less (about 1) for CrIIPt .For the device using Cr for both metal electrodes and with four layer of insulators, the I-V curve was highly asymmetric with value of 16 under voltage of 2volts. Even though this diode consists of the same metal electrodes (Cr), there is still

a work function difference between the two electrodes. The reason of such low barrier height on one side might be due to the difference in processing conditions of electrodes s, as explained by Hobbs [5]. The forward current, which is defined as those electron tunneled from top electrode to the base electrode (Cr), was larger than the reverse current, which is those electrons tunneled from base electrode to top electrode, and hence there is inherent work function difference. Since asymmetry of MIM diode is a function of applied voltage, the amount of voltage bias affects the resulted asymmetry values. Figure.2.8 also shows a low asymmetry using a combination of Cr and Al as base and top electrode, respectively especially for MIIIIM structures at voltage of 1 volt. By applying a voltage bias to Al electrons of the Al tunneled through the thin barrier with a total thickness of 3nm. The amplitude of the current obtained from Cr electrode depends on the barrier heights as well as on the applied voltage. It can be concluded that the increase in asymmetry is not linear function of the work function difference between base and top electrodes which is in good agreement with other studies[2].

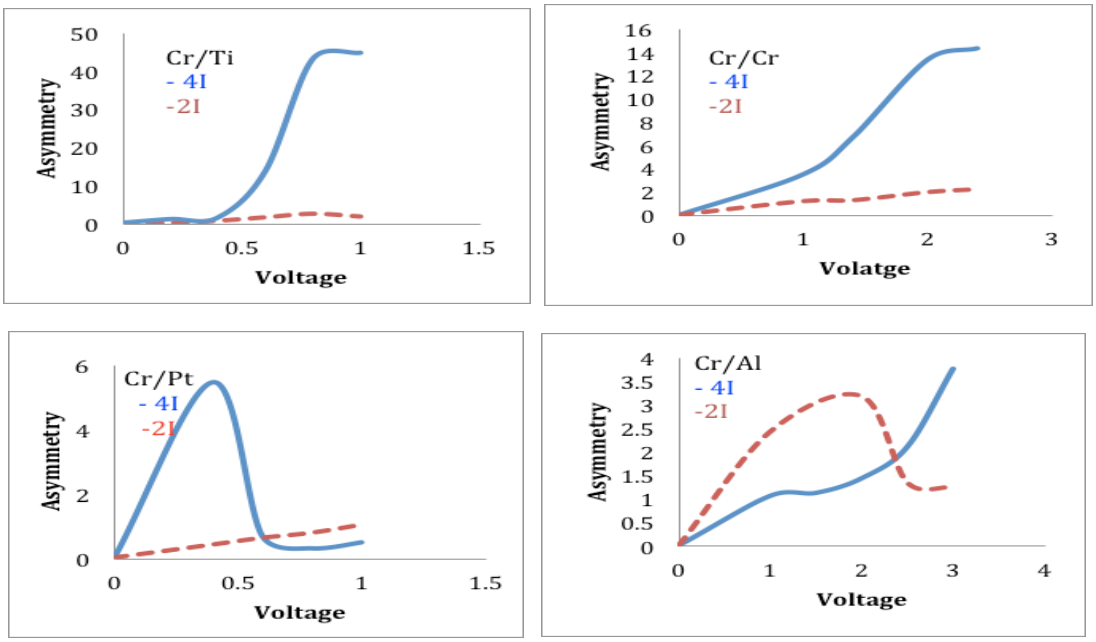

Figure 2.8 Asymmetry curve of the fabricated diodes indicating the two structures MIIM and MIIIIM.

The barrier heights of device's interface were calculated for difference fabricated diodes and were reported in table.1 The electron affinity of 0.75 nm thickness of the TiO_2 and Al_2O_3 was reported as 4.3 eV, and 3.5 eV, respectively. Since each diodes have five interfaces, the barrier heights were calculated as follow: $\Phi_1 = \varphi_1 - \chi_1 = eV$, $\Phi_2 = \Phi_3 = \Phi_4 = \chi_1 - \chi_2$, and $\Phi_5 = \varphi_2 - \chi_2$.

Table.1 Barrier height potential of fabricated MI1I2I1I2M diodes.

MIM#	$\Phi_1=\phi_1-\chi_1$(ev)	$\Phi_2=\Phi_3=\Phi_4=\chi_1-\chi_2$(ev)	$\Phi_5=\phi_2-\chi_2$(ev)
1	0.2	0.8	0.83
2	0.2	0.8	1
3	0.2	0.8	0.78
4	0.2	0.8	2.15

Table.2 shows the list of MIIIIM diodes' various combinations and the differences in work function values between metals one and two. The study of different materials' properties is crucial to determine the suitable material combinations for the optimum metal-insulator-metal diode operation performance.

Table.2 MIIIIM diode combinations and their difference in work function values reported in this study

Metal 1-Insulator 1, 2, 3, 4 – Metal 2 configuration	**Work function difference value Δ φ (= φ 2 – φ 1)**
Cr-Tio_2- Al_2o_3-Tio_2 -Al_2o_3 -Ti	-0.17eV
Cr-Tio_2- Al_2o_3-Tio_2 - Al_2o_3 - Cr	>0eV
Cr-Tio_2- Al_2o_3-Tio_2 - Al_2o_3 -Al	-0.22eV
Cr-Tio_2- Al_2o_3-Tio_2 - Al_2o_3 - Pt	1.15eV

2.2.4 Conclusion

In this work, four new $MI_1I_2I_3I_4M$ diodes were compared following successful fabrication. Characterization of these various diodes was achieved from their I-V electrical responses. MIIIIM diodes using Ti and Cr, and Pt as the second metal electrode exhibited superior performance in terms of asymmetry, while a combination of (Cr –Al) shows relatively lower asymmetry curve.

Chapter 3

Electron Beam Lithography

3.1 Overview of Electron Beam Lithography

Electron beam lithography (EBL) is popular due to its excellent resolution capability, significant reliability, and ability to write reproducible structures over large areas, and low cost. EBL is capable of achieving sub-10nm resolution patterns [17]. EBL, which was generated from scanning electron microscopy (SEM), is a mask less lithography technique since it is only based on the electron beam source. Because electron beam has a small wavelength and small probe size, Electron Beam Lithography has become the most useful nanofabrication tool.

The spot size of electron beam can be less than 5nm, and the beam can be focused using electron optics. However, the literature has reported the general capabilities of different direct lithographies such as (~10 nm) for EBL.

Table 3. Capabilities of different direct nanofabrication techniques [19]

Technology	**Capability**
Optical lithography	~30 nm
Electron beam lithography	~10 nm
Nanoimprint lithography	~10 nm
Scanning probe lithography	~1 nm
Focused ion beam	~30 nm

By using de Broglie wavelength equation, one can estimate the electron wavelength.

$$\lambda = \frac{1.226}{\sqrt{V}} (nm$$

EBL system can resolve a minimum feature size depending on many factors such as resist type, resist thickness, exposure dosage, beam current level, development process, proximity correction, and resistance to etching of the used EBL resist.

3.2 Electron Beam Lithography Systems, Operation, and Working Scheme

3.2.1 Electron Beam Lithography Systems

EBL has different types of systems that have been developed which are used for both research and industry. A schematic of an EBL system is shown in Figure 3.1. Generally, a beam of electrons is deflected to a desired area in the substrate surface. This electron beam modifies the resist depending on its tone by blanking the beam, moving it to another location, and then turning it on in order to expose the resist again. By repeating this process the desired pattern is achieved.

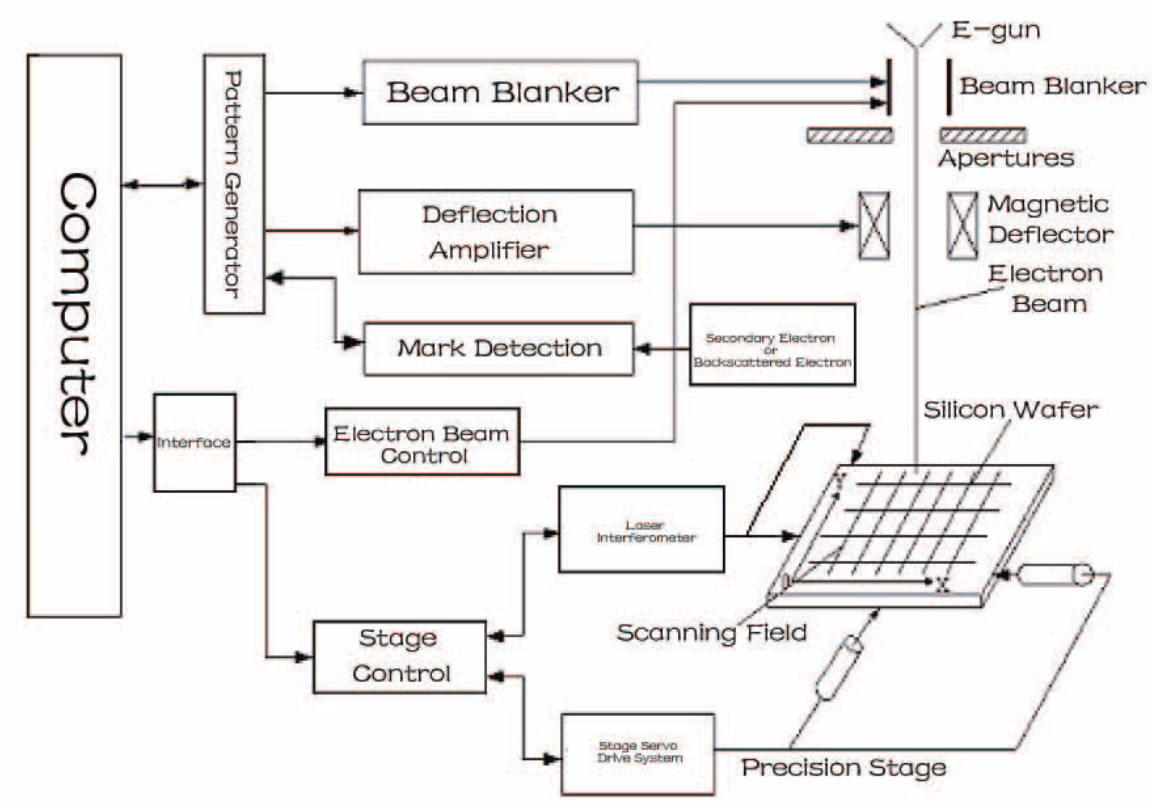

Figure 3.1 EBL System based on SEM [22]

Even though sub-10 nm resolution is achieved by EBL, exposures are done serially which reduces throughput and also limits to the scientific research applications.

Two different types of EBL systems are used for EBL writing: raster and vector scan. In raster scan the electron beam is scanned in only one direction and a mechanical translation of the stage occurs in the perpendicular direction. Unlike raster scan, in vector scan the electron beam is scanned in both x and y directions with beam blanking. Here the pattern writing will be pixel by pixel and without stage movement within each writing field, yet the stage or the substrate will move to the next location after each writing field.

3.2.2 Working Scheme of EBL

An electron beam scans a substrate surface covered with a resist material. This resist material is sensitive to electrons, and is chemically modified depending on its tone. There are two different tones of EBL resists: positive and negative. The positive tone resist is dissolved during the development process, while the negative resist remains, as shown in Figure 3.2.

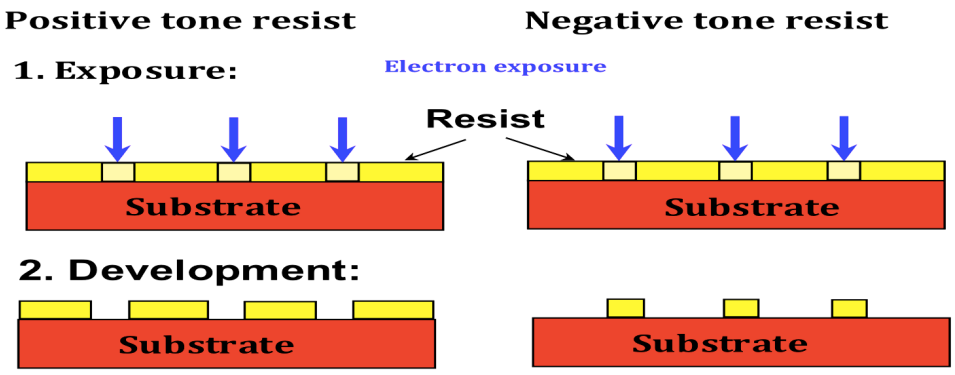

Figure 3.2 A schematic illustration of EBL working scheme

3.3 Proximity Effect

Scattering of the electron beam during exposure leads to pattern distortion. The incident electrons on the resist film cause the resist molecules chains to break.

During the development process, the exposed areas will be dissolvable. When electrons expose undesired areas of the resist, this is called proximity effect. Two scattering events occur: forward scattering and backscattering. In forward scattering event, primary electrons generate secondary electrons along its path but with low energy. However, in backscattering event the resist is exposed far from incidence (proximity effect), because secondary electrons with higher energy and long travel length are generated along backscattered electron path that can expose the resist there.

3.3.1 How to Reduce Proximity Effect

Using thinner resist can minimize the forward scattering. Moreover higher applied voltage can also be used to reduce proximity effect. If it is possible, choosing a substrate with smaller atomic mass unit can be useful. In addition, commercial software can be used to correct the proximity effect by producing a dose-corrected fractured data file.

Chapter 4

Gray Scale Lithography

4.1. Motivation

The second half of this thesis attempts to engineer the contrast curve of electron-beam lithography resist (polystyrene) with a great freedom by using multi-layer of polystyrene. By using multi-layer resist stack, an additional degree of tuning the overall contrast curve is offered.

Successfully designing the resist stack of polystyrene with higher contrast allows it to be used for the fabrication of multi-level zone-plate/Fresnel lens.

4.2. Overview of Gray Scale Lithography

In EBL, resist properties are characterized by sensitivity and contrast which can be derived from its contrast curve. To a certain degree, resist sensitivity and contrast can be tailored by experimental parameters. For example, for positive resist such as PMMA, using lower electron beam energy can increase the sensitivity or stronger concentration of the developer (e.g. MIBK:IPA=1:1, instead of 1:3) and increase the development temperature or the development time. The dependence of contrast on those parameters is not obvious, but for typical resist increased sensitivity is always accompanied by decreased contrast. Nonetheless, the tailoring of the contrast curve using single resist layer is limited. It is proposed that by using polystyrene with different molecular weights

(Mw), a multi-layer resist stack can be designed in order to engineer the contrast curve of the stack with great freedom.

Polystyrene is chosen because its sensitivity is proportional to its Mw [12, 14], which is commercially available from ~1 kg/mol up to 2000 kg/mol. Moreover, it is not necessary to have polystyrene with many different Mw, as one can "simulate" an arbitrary Mw (actually should be Mn, number averaged molecular weight, which is more important than weight averaged molecular weight Mw) by mixing two polystyrenes with very different Mw [15]. As shown schematically in Figure 4.4, if the resist layers have very high contrast - which is the case for low Mw range polystyrene - and the sensitivity of the layers differ greatly from each other, a contrast curve with roughly a stair-case shape may be achieved, which is ideal for the fabrication of multi-level zone-plate/Fresnel lens [16].

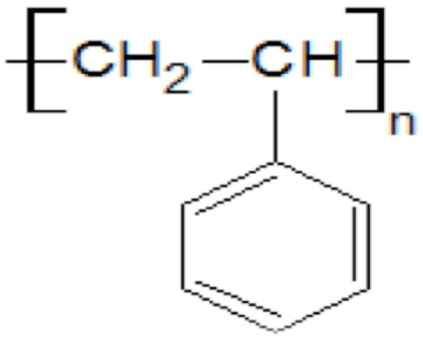

Figure 4.1 Chemical structure of Polystyrene

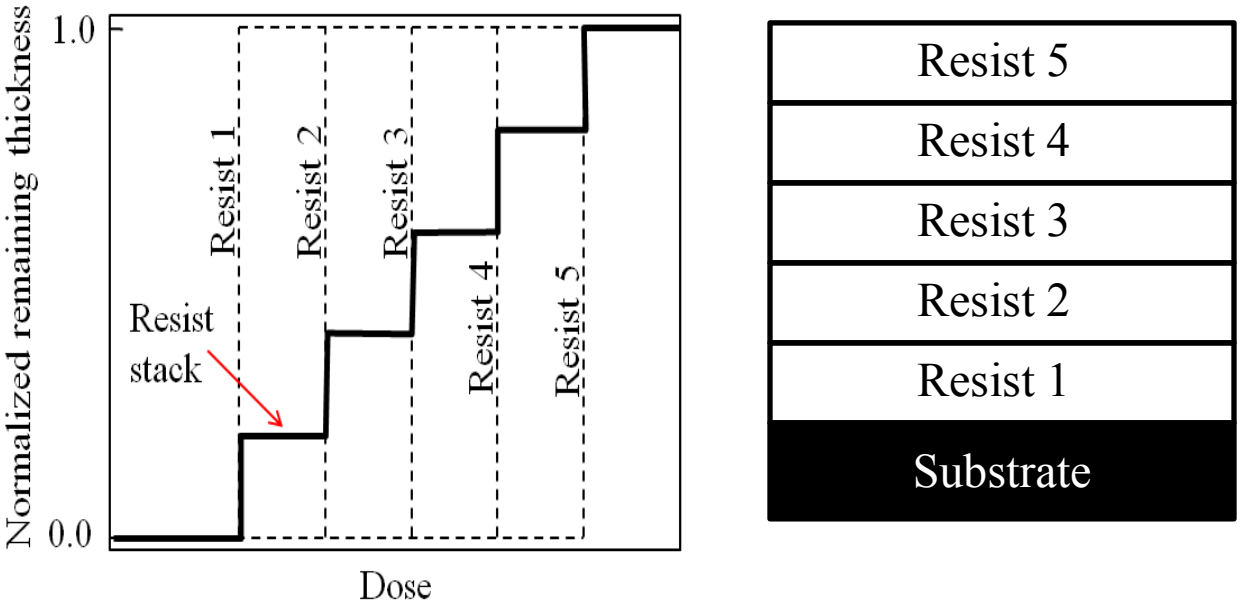

Figure 4.2 Schematic of contrast curves of five high contrasts resists having decreasing sensitivity, as well as the contrast curve for the stack of the five resists (most sensitive on bottom and least sensitive on top)

4.3. Experimental

4.3.1 Doubled-layer Resist Stack

In the experiment, two PS samples with Mw of 50 kg/mol and 4.5 kg/mol were used. Two grams of PS of Mw of 50 kg/mol were dissolved in 100ml toluene solvent. Another 2g of PS of Mw of 4.5 kg/mol were dissolved in 100ml toluene solvent. A third solution of 22 kg/mol was prepared by mixing the previous two samples of 50 and 4.5 kg/mol. Spin coating of 50 kg/mol solution was applied on bare Si wafer, and 22 kg/mol solution was spin coated on another Si wafer. Before exposure, the films were baked for one minute for hardening after the spin coating step. Dektak-8 program was used to check the thickness of the two films. The pattern was exposed at 20kev and 320 PA beam current and developed using xylene for one minute. After development, the remaining thickness was measured by AFM.

A straightforward way to generate the resist stack is by spin coating the polystyrene layer by layer. However, this has not yet been successful because it was found that the solvent dissolved the previous layers during the coating of a new layer. It is known that double-layer PMMA can be spin coated; thus, the same may be possible for polystyrene if a suitable solvent or mixture of solvents can be identified. As proof of concept, a double layer of polystyrene was obtained by thermally bonding one layer to the other, with the first layer spin coated on a bare silicon wafer and the second layer spin coated on an anti-adhesion treated wafer, as shown in Figure 4.3.

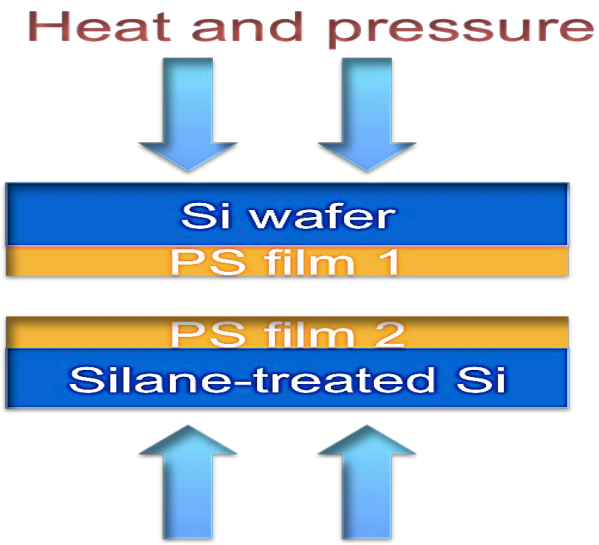

Figure 4.3 A schematic representation of thermal bonding of Ps layers

The contrast curve of two-layer stack, 22 kg/mol on top of 50 kg/mol, is shown in Figure 4.4. Here the effective 22 kg/mol is simulated by a mixture of 50 kg/mol and 4.5-kg/mol polystyrene. Due to the small difference between the two Mw, the contrast curve has a continuous and smooth slope, yet the contrast is decreased to 2.0 which is lower than the single layer resist with similar Mw (γ~3.0).

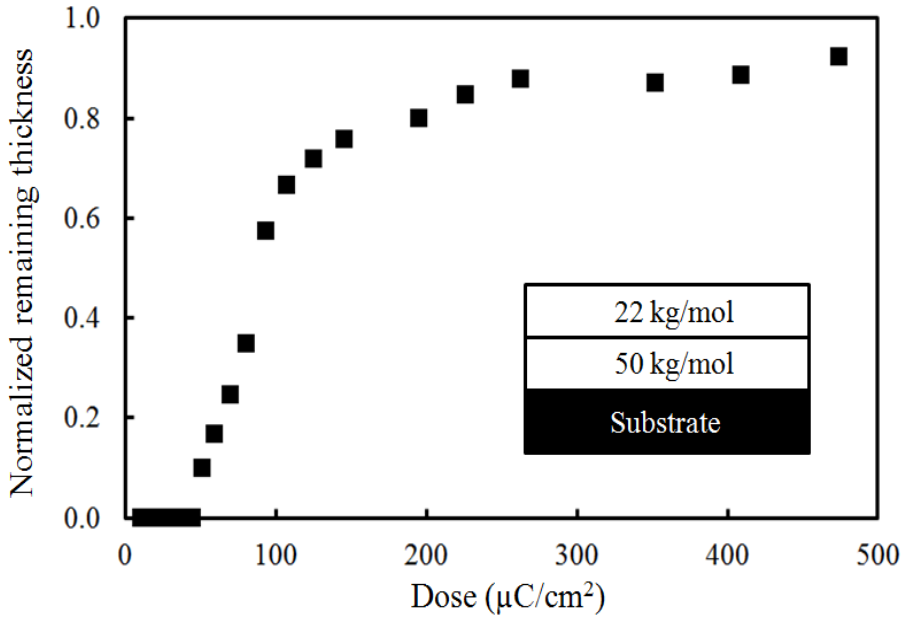

Figure 4.4 Contrast curve for a two-layer polystyrene resist stack, with each layer ~180 nm thick. Here 22 kg/mol is a calculated effective Mn for a mixture of 4.5 kg/mol and 50 kg/mol polystyrene exposed at 20 keV, and resist height measured by AFM.

In this experiment, polystyrene was dissolved in toluene in order for it to be spin-coated on silane-treated wafer having low surface energy. Two polystyrene films were bonded using a home-built thermal nanoimprint tool at 130^{o}C and 100psi pressure for 30 min. After thermal bonding, exposure was carried out using Raith 150^{TWO} at 10 or 20 keV. Next, development was achieved using xylene for 1-2 min, followed by IPA rinse and nitrogen blow-drying. Finally, contrast curve was acquired by AFM measurement.

4.3.2 Tri-layer Resist Stack

A tri-layer resist stack was fabricated using polystyrene with three different Mn. The bottom layer has a number averaged molecular weight (Mn) of 64kg/mol and weight averaged molecular

weight of 282kg/mol (see Figure 4.5). Figure 4.7 clearly shows the two steps. Mn dominates exposure properties.

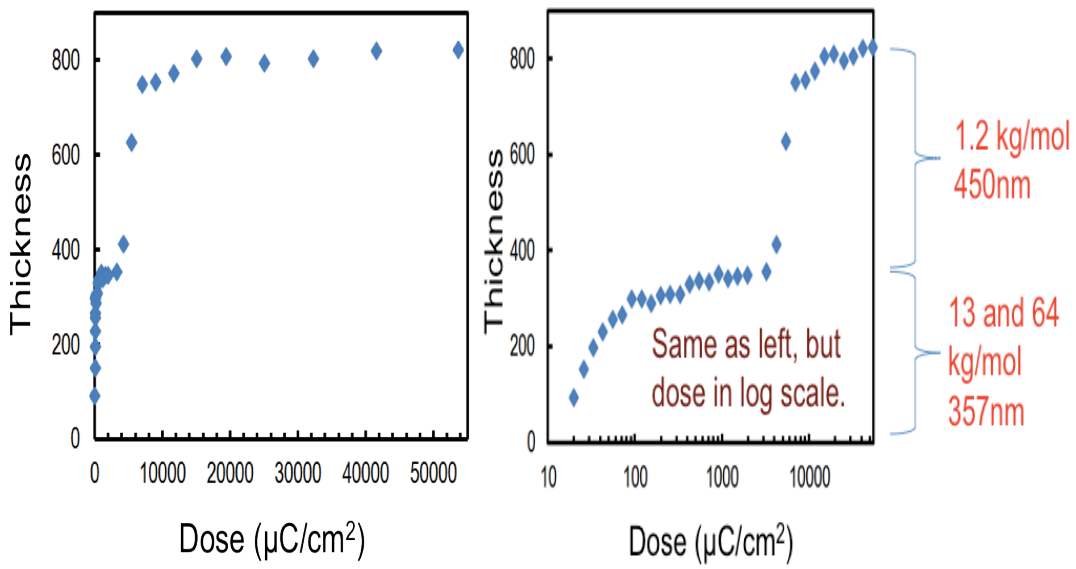

Figure 4.5 Contrast curve at 10keV for tri-layer polystyrene, with bottom two layers by thermal bonding and the top layer subsequently coated by thermal evaporation of 1.2 kg/mol polystyrene

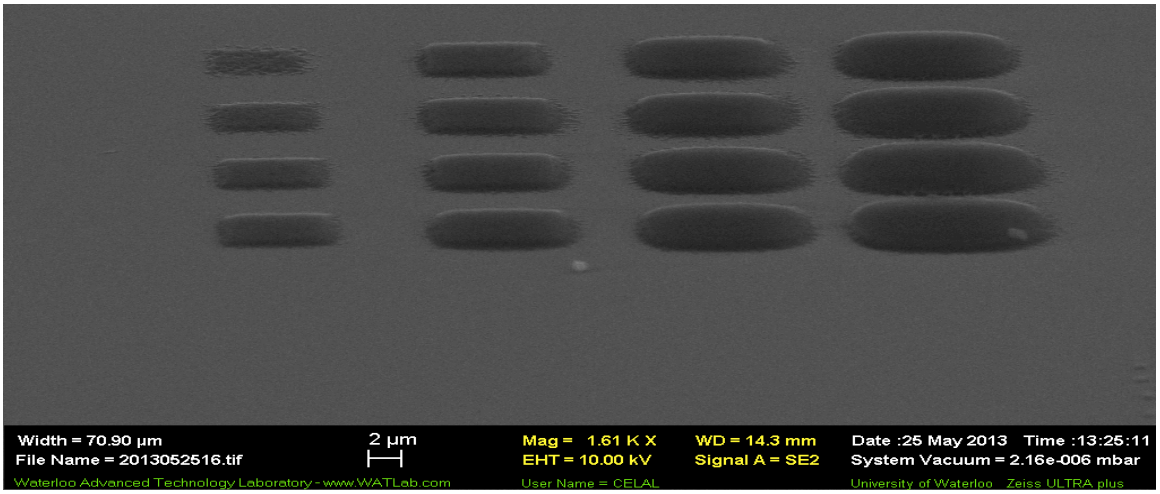

Figure 4.6 SEM image of exposed square patterns

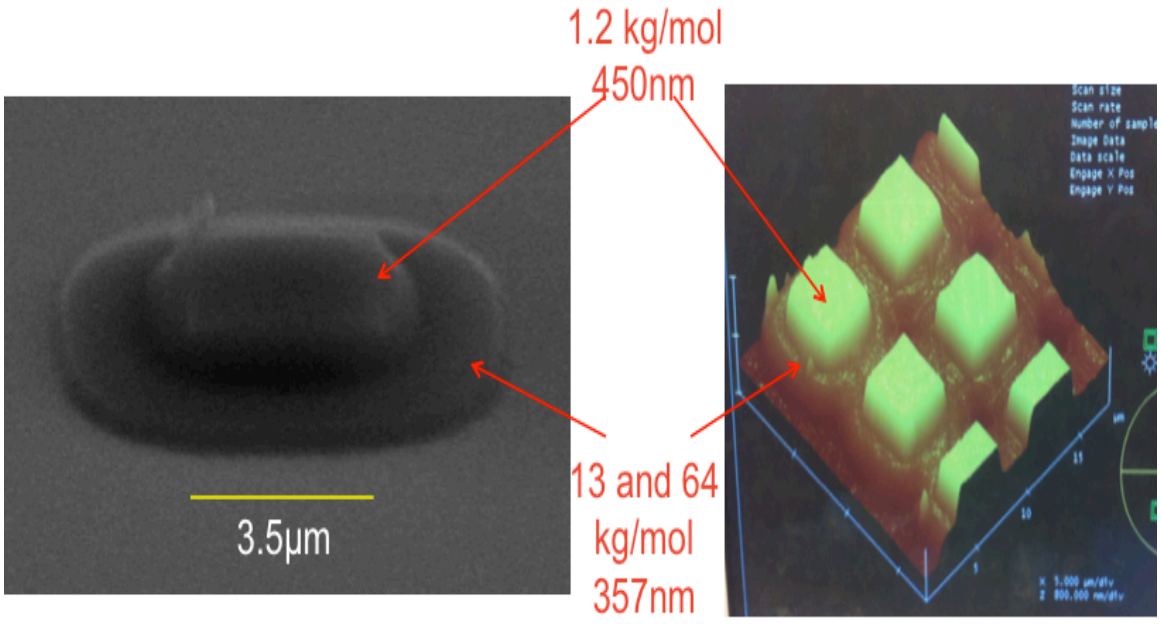

Figure 4.7 SEM and AFM images of exposed square patterns which clearly show the two steps. The square is 3.5μm in the CAD file. The larger square for the bottom two layers is due to proximity over-exposure.

To validate the results, a four-layer stack of polystyrene was achieved using thermal bonding technique. First, polystyrene with different numbers of averaged molecular weight was dissolved in toluene. Each polystyrene film had a thickness of 200-300nm. The first polystyrene film with Mn of 170 kg/mol was spin coated on a bare Si wafer, while the second film with Mn of 64 kg/mol was spin coated onto a PEN sheet coated with a fluorocarbon film. The two polystyrene films were bonded using a home-built thermal nanoimprint tool at 130^{o}C and 100psi pressure for 30 min. Reactive ion etching RIE was used to coat fluorocarbon film on PEN sheet in order to facilitate the separation of the two polystyrene films after bonding. By repeating the process of spin coating and thermal bonding using polystyrene films with Mn of 18 kg/mol and 6 kg/mol, one can achieve four layers of polystyrene with different weight averaged molecular weight (Figure 4.8). Exposure was carried out using Raith 150^{TWO} at 20 keV. Next, development was

achieved using xylene for 3 min followed by IPA rinse and nitrogen blow-drying. Finally, contrast curve was acquired by AFM measurement, as shown in Figure 4.10.

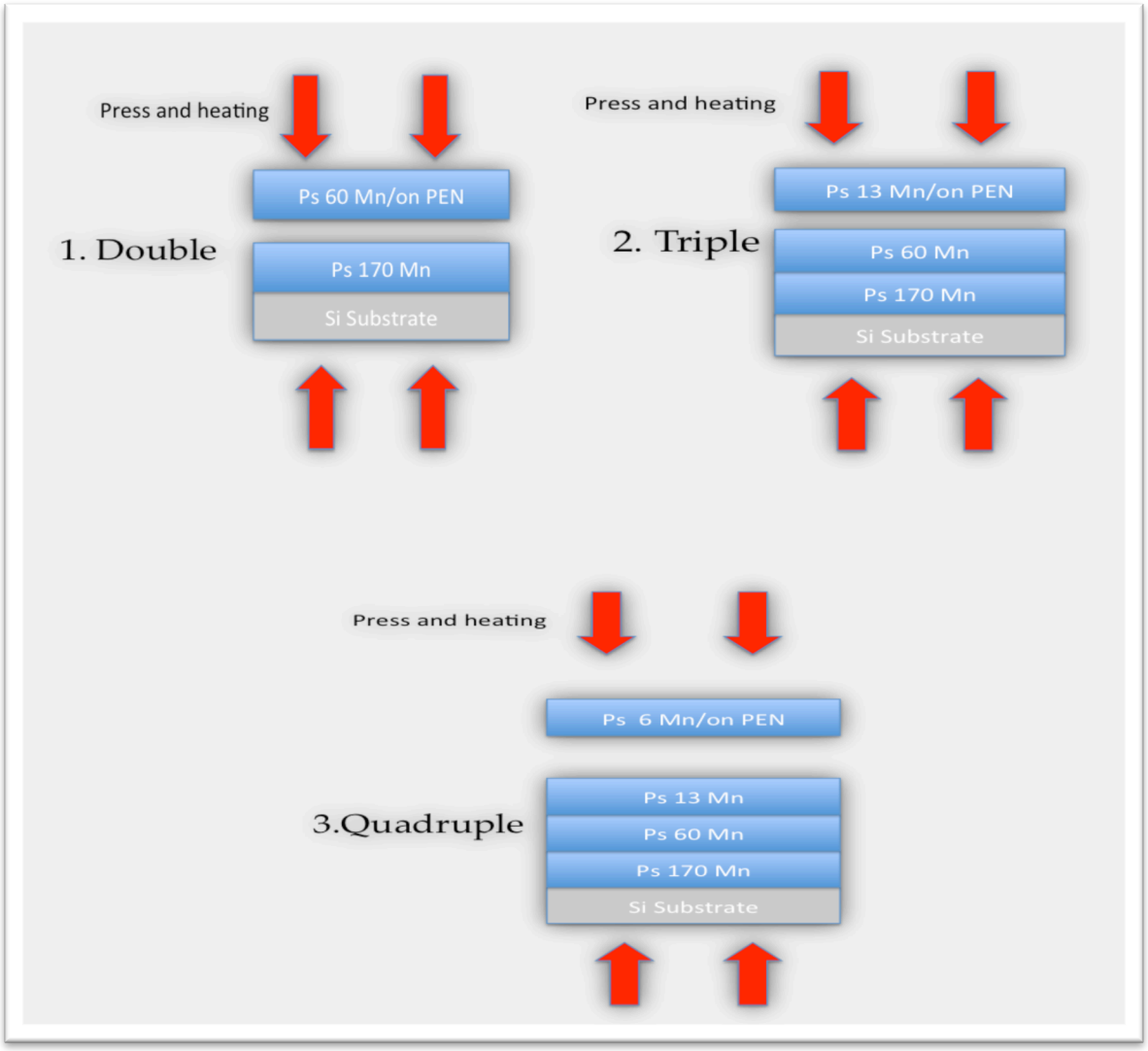

Figure 4.8 Schematic representation of thermal bonding process of the four polystyrene films where weight averaged molecular weight is in the following order: (Mw1>Mw2>Mw3>Mw4)

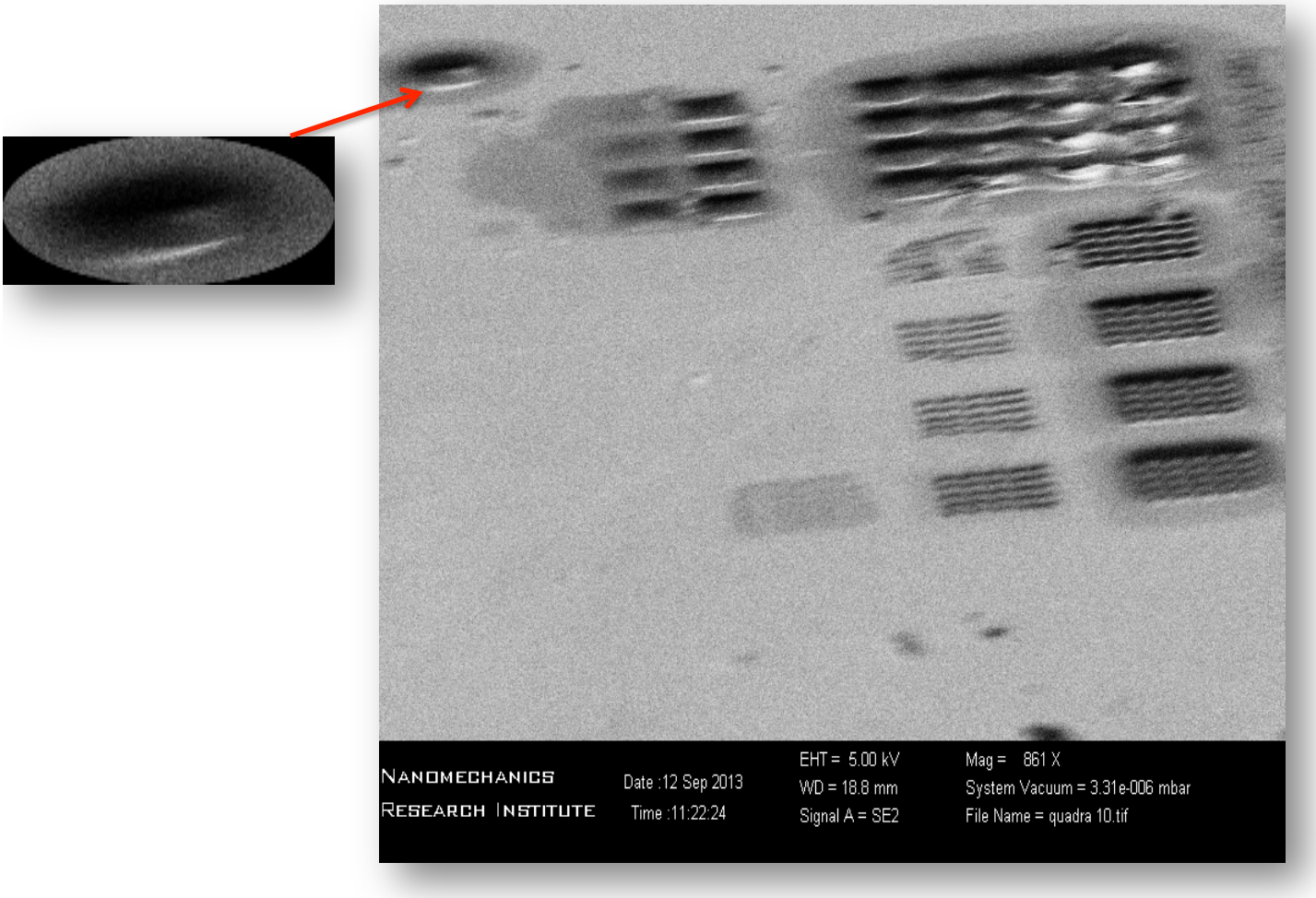

Figure 4.9 SEM images of the exposed square patterns showing the height of the resist corresponding to the film thickness

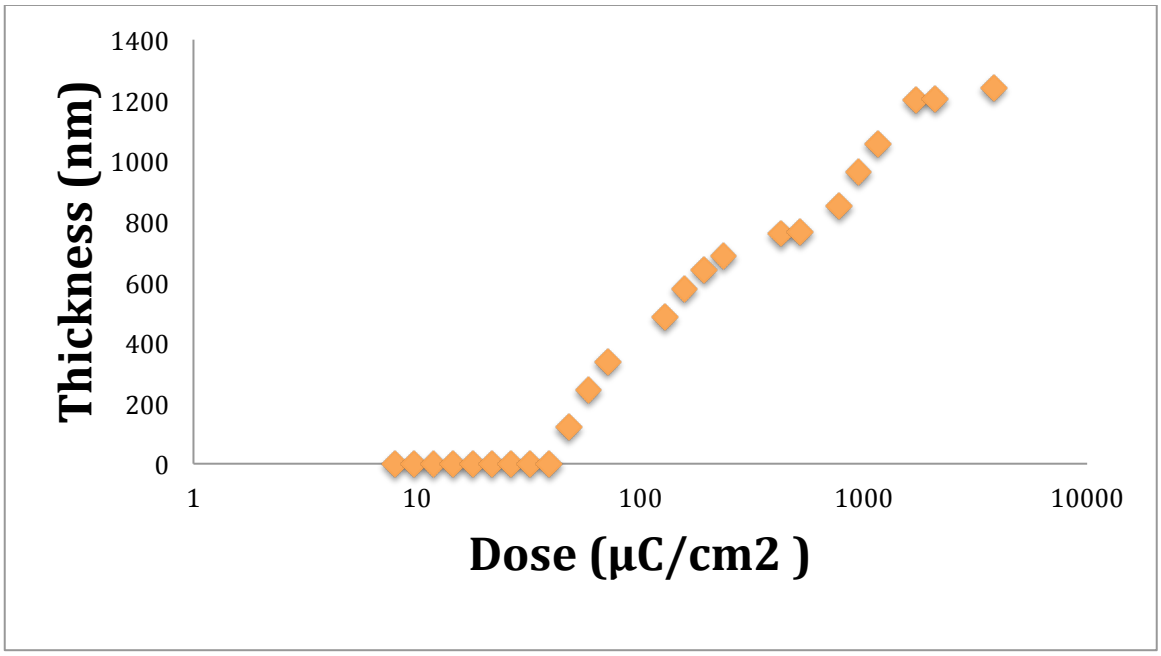

Figure 4.10 Contrast curve of the four-layer resist stack using polystyrene as negative resist

4.5 Fresnel Lenses

A Fresnel lens is a thin light magnifier that can be used as an alternative to the conventional continuous surface lens. Augustin Jean Fresnel developed this type of lens in the early 1800s. Due to its structure that becomes flat in one side and ridged on the other, Fresnel lens is cost effective, with much of the optical material removed and the surface curvature still being maintained. This concept is illustrated in Figure 4.11.

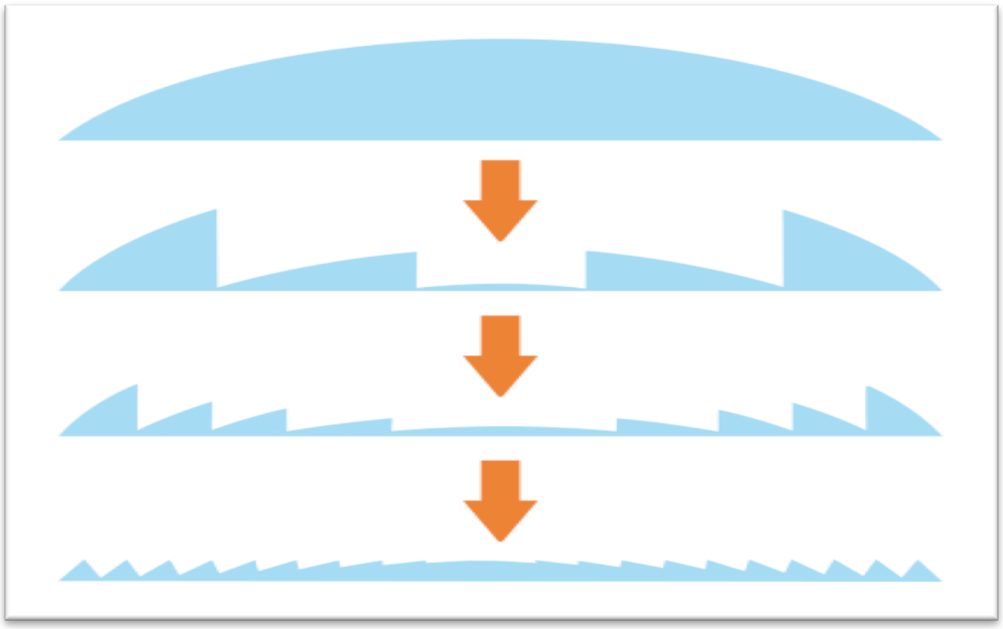

Figure 4.11 Conceptual illustration (in side-profile) of collapsing a continuous surface aspheric lens into an equivalent power Fresnel lens [18]

Appendix

List of Publications

Papers

1. M. Alhazmi, M. Yavuz and B. Cui, Contrast curve engineering by using multi-layer polystyrene electron beam resist, 57th International Conference on Electron, Ion and Photon Beam Technology and Nano-fabrication (EIPBN), Nashville, May 2013.

2. M. Alhazmi, F. Aydinoglu, B. Cui, O. M. Ramahi, M. Irannejad, A. Brzezinski and M. Yavuz, "Comparison of various materials properties effect on metal-insulator-metal diodes", *under preparation for submission.*

3. F. Aydinoglu, M. Alhazmi, S, Alqarni, B. Cui, O.M. Ramahi, M. Yavuz, Design and fabrication of pt-al_2o_3-al metal-insulator-metal diode, 24th Canadian Congress of Applied Mechanics (CANCAM), Saskatoon, SK, Canada, 2nd June, 2013.

4. C. Con, M. Alhazmi, M. yavuz and B. cui, freeze-drying for the reduction of e-beam resist collapse, MNE conference in London (UK), September 2013

5. F. Aydinoglu, M. Alhazmi, B. Cui, O. M. Ramahi, M. Yavuz, "Higher Performance Metal-Insulator-Metal Diodes using Multiple Insulator Layers" *Applied Physics Letters* (under review, Sep 2013.

Conference presentations

1- M. Alhazmi, M. Yavuz and B. Cui, Contrast curve engineering by using multi-layer polystyrene electron beam resist, 57th International Conference on Electron, Ion and Photon Beam Technology and Nano-fabrication (EIPBN), Nashville, May 2013.

2- F. Aydinoglu, M. Alhazmi, S, Alqarni, B. Cui, O.M. Ramahi, M. Yavuz, Design and fabrication of pt-al_2o_3-al metal-insulator-metal diode, 24th Canadian Congress of Applied Mechanics (CANCAM), Saskatoon, SK, Canada, 2nd June, 2013.

Bibliography

[1]Eliasson, B. 2001, “Metal –Insulator-Metal diodes for solar energy conversion”, University of Colorado, Boulder, Doctoral thesis.

[2]B. H. Strassner and K. Chang.2005, “Rectifying antennas (rectennas),” in Encyclopedia of RF and Microwave Engineering. Hoboken, NJ: Wiley, p. 4418.

[3]Grover, S., Moddel, G. 2011, "Applicability of Metal/Insulator/Metal (MIM) Diodes to Solar Rectennas", IEEE Journal of Photovoltaics, Vol.1 (1), pp.78-83.

[4]Da Costa V., Romeo, M., Bardou, F. 2003, "Statistical properties of currents flowing through tunnel junctions", Journal of Magnetism and Magnetic Materials, Vol.258–259, pp. 90-95.

[5]Grover, S., Dmitriyeva, O., Estes, M.J., Moddel, G. 2010, "Traveling-Wave Metal/Insulator/Metal Diodes for Improved Infrared Bandwidth and Efficiency of Antenna-Coupled Rectifiers", IEEE Transactions on Nanotechnology, Vol.9 (6), pp. 716-722.

[6]Choi, K., Dagenais, M., Peckerar, M. 2009, “Fabrication of Thin Film Asymmetric Tunneling Diode using Geometric Field. Enhancement”, Semiconductor Device Research Symposium, ISDRS '09. International, College Park, MD, USA.

[7]Krishnan, S., La Rosa, H., Stefanakos, E., Bhansali, S., Buckle K. 2008, "Design and development of batch fabricatable metal–insulator–metal diode and microstrip slot antenna as rectenna elements”, Sensors and Actuators A: Physical, Vol.142 (10), pp. 40-47.

[8] Dagenais, M., Choi, K., Yesilkoy, F., Chryssis, A., Peckerar, M. 2010, "Solar spectrum rectification using nano-antennas and tunneling diodes", Optoelectronic Integrated Circuits XII. Edited by Eldada, Louay A. Lee, El-Hang. Proceedings of the SPIE, Vol.7605, pp. 76050E-76050E-12.

[9] Krishnan, S., 2004 “Design, Fabrication and Characterization of Thin-Film M-I-M Diodes for Rectenna Array", University of South Florida, Florida, Master Thesis.

[10] S., Stefanakos, E., Bhansali, S. 2008, “Effect of dielectric thickness and contact area on current-voltage characteristics of thin film metal-

[11] Hashem, I.E.; Rafat, N.H.; Soliman, E.A., 2013, "Theoretical Study of Metal-Insulator-Metal Tunneling Diode Figures of Merit", IEEE Journal of Quantum Electronics, Vol.49 (1), pp. 72-79.

[12] H. Y. Ku and L. C. Scala, J. Electrochem, 1969,Soc., 116, 980.

[13] C. Con, R. K. Dey, M. Ferguson, J. Zhang, R. Mansour, M. Yavuz and B. Cui, 2012, Microelectron. Eng., 98, 254.

[14] S. Ma, C. Con, M. Yavuz and B. Cui, 2011, Nanoscale Research Letters, 6, 446.

[15] R. K. Dey and B. Cui, presented at EIPBN 2012, and manuscript submitted.

[16] E. D. Fabrizio, F. Romanato, N, Gentili, S. Cabrini, B. Kaulich, J. Susini and R. Barrett, 1999, Nature, 401, 895.

[17] Grigorescu, A. E. and Hagen, C. W. 2009. Resists for sub-20-nm electron beam lithography with a focus on HSQ: state of the art. Nanotechnology, **20**, 292001

[18] P. University. *Scanning Electron Microscope*.Accessed on September 10th,2013. http://www.purdue.edu/rem/rs/sem.htm

[19] Cui, Z. (2008). Nanofabrication. doi: 10.1007/978-0-387-75577-9

[20] L. Reimer and C. Tollkamp, 1980,"Measuring the Backscattering Coefficient and Secondary-Electron Yield inside a Scanning Electron-Microscope," *Scanning,* vol. 3, pp. 35-39.

[21] G. Messina, A. Paoletti, S. Santangelo, and A. Tucciarone,Feb 1995, "A Single Quality Factor for Electron Backscattering from Thin-Films," *Microelectronic Engineering,* vol. 27, pp. 183-186.

[22] Shuhua, W., Lan, D., & Jing, Z. 2013, Realization and application of nanometer E-beam lithography system. *IEEE 5th International Nanoelectronics Conference (INEC)*, (5), 164–167. doi: 10.1109/INEC.2013.6465985.

[23] J. Y. Liu, 2000."High-resolution and low-voltage FE-SEM imaging and microanalysis in materials characterization," *Materials Characterization,* vol. 44, pp. 353-363.